Ocean Dynamics (2008) 58:441–460
DOI 10.1007/s10236-008-0163-4

# A multigrid methodology for assimilation of measurements into regional tidal models

**Oleg G. Logutov**

Received: 14 May 2008 / Accepted: 2 November 2008 / Published online: 20 November 2008


**Abstract** This paper presents a rigorous, yet practical, method of multigrid data assimilation into regional structured-grid tidal models. The new inverse tidal nesting scheme, with nesting across multiple grids, is designed to provide a fit of the tidal dynamics to data in areas with highly complex bathymetry and coastline geometry. In these areas, computational constraints make it impractical to fully resolve local topographic and coastal features around all of the observation sites in a stand-alone computation. The proposed strategy consists of increasing the model resolution in multiple limited area domains around the observation locations where a representativeness error is detected in order to improve the representation of the measurements with respect to the dynamics. Multiple high-resolution nested domains are set up and data assimilation is carried out using these embedded nested computations. Every nested domain is coupled to the outer domain through the open boundary conditions (OBCs). Data inversion is carried out in a control space of the outer domain model. A level of generality is retained throughout the presentation with respect to the choice of the control space; however, a specific example of using the outer domain OBCs as the control space is provided, with other sensible choices discussed. In the forward scheme, the computations in the nested domains do not affect the solution in the outer domain. The subsequent inverse computations utilize the observation-minus-model residuals of the forward computations across these multiple nested domains in order to obtain the optimal values of parameters in the control space of the outer domain model. The inversion is carried out by propagating the uncertainty from the control space to model tidal fields at observation locations in the outer and in the nested domains using efficient low-rank error covariance representations. Subsequently, an analysis increment in the control space of the outer domain model is computed and the multigrid system is steered optimally towards observations while preserving a perfect dynamical balance. The method is illustrated using a real-world application in the context of the Philippines Strait Dynamics experiment.

**Keywords** Tidal modelling · Inverse methods · Nesting

Responsible Editor: Eric Deleersnijder

O. G. Logutov (✉)
Massachusetts Institute of Technology,
77 Massachusetts Ave., rm. 7-321,
02139 Cambridge, MA, USA
e-mail: logutov@mit.edu

## 1 Introduction

A significant number of tidal observations are collected along coasts and in inland waterways with complex coastline geometry and bottom topography. Local small-scale coastal and topographic features are often consequential for the tidal fields measured at coastal locations. For example, coastal measurements in (semi)enclosed bays and estuaries might not be representative of the nearby open-ocean areas, but rather reflect the local characteristics of the shoreline. On the other hand, the computational constraints limit model resolution and often lead to an insufficient representation of small-scale coastal and topographic features

in areas where measurements are obtained, such as estuaries, channels, and sills. This presents a difficulty with respect to the assimilation of measurements into regional tidal models. The measurements utilized for assimilation must be representative of the tidal dynamics at a model resolution. An artificial steering of the solution towards unresolved observations can be counter-productive and lead to a degradation of model accuracy. With the unstructured grid tidal models, the mesh resolution can be selectively adjusted around all of the observation locations to fully resolve important coastal features. The structured grid tidal models are less conducive to selective resolution adjustments and, therefore, part of the observational network might be unresolved. A popular way of avoiding the difficulty within the structured grid modeling framework is either an exclusion of the unresolved measurements from the data set or an inflation of the representativeness error covariance around coastal segments unresolved in a model. Both approaches lead to a loss of information from part of the observational network.

The present paper describes a new multigrid data assimilation scheme for regional tidal modeling applications that provides a rigorous way of reducing the representativeness error by employing a multigrid, data-assimilative framework. The representativeness error can be detected by analyzing the observation-minus-forecast residuals and their sensitivity to model resolution. Adaptive methods for data assimilation reviewed in Lermusiaux (2007) can potentially be useful for distinguishing the error of representativeness due to model and bottom topography resolutions vs that due to model formulation. If data-model misfits are found to be consistently larger than the average in certain areas of model domain, the representativeness component in these misfits can be analyzed through refinements to model grid resolution. If misrepresentation due to insufficient resolution is detected, it can be dealt with in the data assimilative component of the modeling system by using the method presented in this paper. High-resolution nested domain(s), coupled to the outer model domain via the open boundary conditions (OBCs), can be setup around the problematic areas and the assimilation can be carried out using these nested computation(s). Thus, with the use of the nested domains, coastal measurements can be assimilated into a modeling system consistently with the resolution. A real-world example of such an application in the context of the Philippines Straits dynamics experiment (PhilEx) is discussed in Section 5 as a demonstration.

An extensive variety of methods exist to constrain regional barotropic tidal estimates with the observational tidal elevation and velocity data (Egbert and Bennett 1996; Robinson and Lermusiaux 2001; Lermusiaux et al. 2006b). The techniques differ by the choice of an optimization space and by the specifics of implementation. An early important contribution included a variational formulation developed by Bennett and McIntosh (1982) which led to the adjoint techniques of generalized inverse tidal solution, subsequently utilized in a variety of tidal applications (*e.g.* McIntosh and Bennett 1984; Egbert 1997; Muccino et al. 2008). The representer method (Bennett 1992, 2002) and its reduced-basis alternatives (Egbert and Erofeeva 2002) have been developed following this approach and successfully applied to assimilation of Topex/Poseidon altimeter data (Egbert et al. 1994), estimation of the internal tides (Kurapov et al. 2003), and in other coastal ocean modeling applications (Muccino et al. 2008). The aforementioned methods have one feature in common, namely, an optimization is carried out in the (reduced) data space and requires an adjoint tidal model. Alternative techniques that do not require an adjoint model have also been proposed. These include the steady-state Kalman filter (KF) schemes (Heemink and Kloosterhuis 1990; Sorensen and Madsen 2004) that carry out an optimization in the model state space and rely on reduced-rank error covariance models, defined in the model state space, evolved using stochastic linearized shallow water equations. The KF-based schemes were utilized in a series of realistic two-dimensional inverse problems arising from the assimilation of water level measurements into a regional model of the North Sea (Sorensen and Madsen 2004) and a storm surge prediction model of Danish coastal waters (Canizares et al. 2001). Lynch and Hannah (1998), Xu et al. (2001), and Logutov and Lermusiaux (2008) have developed an inverse scheme that carries out an optimization in the OBC space, also without the need of an adjoint model. The method was specifically developed for regional tidal modeling applications and successfully applied near the Georges Bank, near the Newfoundland and South Labtador shelves, and off the coast of Vancouver Island and in the Hood Canal and Dabob Bay region of WA (Xu et al. 2008), as well as in other regions (Haley et al. 2008). Nudging and optimal interpolation schemes have been proposed and applied in some tidal modeling systems, *e.g.*, Navy PCTides system (Hubbert et al. 2001). Adjoint schemes that utilize bottom topography or model parameters as the control space have also been proposed (*e.g.*, Das and Lardner 1992) but not yet fully demonstrated in real-world applications.

A variety of structured and unstructured grid tidal models are currently in use across various organizations (Davies et al. 1997). The finite-difference

(*e.g.*, LeProvost and Vincent 1986; Davies 1993), the finite-element (*e.g.* Jones and Davies 1996; Walters 2005; Greenberg et al. 2005), and the structured nonorthogonal curvilinear coordinate (*e.g.* George 2007) schemes have been proposed and developed into stand-alone computational systems for regional tidal modeling. Jones and Davies (2005) provide intercomparison between the finite-difference and the finite-element schemes using an example of tidal modeling in the Irish sea. An advantage of the unstructured grid approach is efficiency in representing complex boundary geometries and the potential of employing higher-order approximation schemes, for example, the high-order discontinuous Galerkin method discussed in Bernard et al. (2008). As a result, the unstructured grid tidal models can be made representative of tidal measurements even in areas with complex boundary geometries. However, the generation of unstructured grids, especially for time domain models, is a difficult and time-consuming task that requires considerable human intervention and experience (Blain et al. 2002). In addition, the unstructured grid models are more prone to contamination of the solution with spurious gravity-wave modes, while the finite-difference schemes can be easily made to contain no spurious modes (Walters 2005). For these and other reasons, structured-grid tidal models remain an important component of tidal prediction in both operational and research settings. As an example, the US Navy tidal prediction system currently consists of a time domain finite-element barotropic tidal model ADCIRC (Luettich et al. 1992) and a finite-difference spectral model PCTides (Hubbert et al. 2001). The finite-element system is limited to a number of preexisting computational meshes and is not as easily relocatable as the PCTides system, which provides a rapidly relocatable capability and can be quickly exercised in any region of the world (Blain et al. 2002).

The purpose of this article is to present a rigorous, yet practical, method of data assimilation into regional structured grid tidal models that allows for the use of nested domain(s) resolving the tidal dynamics near the observations that are otherwise unresolved and contain a representativeness error. The computational constraints often make it impractical to fully resolve local topographic and coastal features around all of the observation sites in stand-alone structured grid models. A general discussion of the sensitivity of regional tidal solutions to mesh resolution is provided by Jones and Davies (2007a, b), Walters (2005), Jones and Davies (1996), and LeProvost et al. (1994). The proposed strategy consists of increasing the model resolution in limited-area nested domains in order to improve the representation of the measurements with respect to the dynamics. In our method, the nested domains are coupled to the outer domain via the OBCs. In the forward system, the computations in the nested domains do not affect the solution in the outer domain, while in the inverse system, observation-minus-forward model residuals computed in the nested domains affect the solution in the outer domain. Data inversion is carried out in a control space of the outer domain model. An adjoint model is not needed in the method because of the low-rank formulation adopted for the representation of the error covariance of the control parameters. The presented approach is tailored towards the applications where the use of strong model constraints is desirable. The multigrid system is steered towards observations via the control parameters of the outer domain model (*e.g.*, OBCs of the outer model) and the inverse solution preserves a perfect dynamical balance. An alternative strategy and a sequential scheme for weakly constrained estimation across nested domains using a KF approach is presented in Barth et al. (2007). The authors have proposed an analysis scheme that uses a single multivariate state vector comprised of the variables from multiple nested models that leads to a reduction of the inconsistencies along the nesting boundaries.

The presence of the representativeness error can, in general, be detected through the sensitivity experiments with model resolution. If the observation-minus-model residuals have a consistent bias in certain areas of the domain and this bias is found sensitive to model resolution, the representativeness error can be suspect. In this case, high-resolution nested domain(s) can be setup around such areas and the assimilation in those areas can be carried out using the nested computation(s). Thus, the representativeness error can be reduced and coastal measurements can be assimilated into a multigrid modeling system more consistent with the resolution.

The organization of this paper is as follows. In Section 2, the model equations, both in continuous and discrete formulations, are described. The model formulation presented is a specific example of the dynamical constraints of the inverse scheme. It is provided here only as an illustration for clarity. Importantly, the method can be extended to use with other structured grid tidal models. Section 3 presents the proposed multigrid assimilation method, with a subsequent discussion in Section 4. Finally, an illustration of the methodology in the context of the Philippines Strait dynamics experiment is presented in Section 5. The goal in Section 5 is not a comprehensive description of tidal dynamics in the Philippines basin but rather an

illustration and an analysis of the described method, as applied in realistic settings. The Appendix outlines the index notation utilized in Section 2.

## 2 Model formulation

### 2.1 Dynamical equations

The governing equations that we utilize as the dynamical constraints of the inverse scheme consist of the shallow water equations forced through the OBCs. In coastal applications, the self-attraction and loading terms, as well as the direct astronomical forcing, are negligible as compared to the open boundary forcing and can be omitted from the equations (Snyder et al. 1979). The development presented here consists of the depth-averaged equations. The 2-D formulation allows us to remove a layer of complexity related to parametrization of the vertical divergence of Reynolds stresses in the momentum equations required in the 3-D models. However, an extension to a 3-D formulation is straightforward if needed. In differential form, the governing equations are expressed in spherical coordinates $(\lambda, \phi)$, where $\lambda$ and $\phi$ are the longitude and the latitude, respectively, using the linearized barotropic shallow water equations

$$\frac{\partial}{\partial t}\eta + \frac{1}{a\cos\phi}\frac{\partial}{\partial\lambda}(Hu) + \frac{1}{a\cos\phi}\frac{\partial}{\partial\phi}(Hv\cos\phi) = 0$$

$$\frac{\partial}{\partial t}u - fv + \kappa u = \frac{-g}{a\cos\phi}\frac{\partial}{\partial\lambda}\eta \tag{1}$$

$$\frac{\partial}{\partial t}v + fu + \kappa v = \frac{-g}{a}\frac{\partial}{\partial\phi}\eta$$

subject to the zero normal flow condition

$$\mathbf{n}\cdot\mathbf{u}\Big|_{\partial\Omega_C} = 0 \tag{2}$$

at closed boundaries, and the Dirichlet conditions

$$\eta\Big|_{\partial\Omega_O} = \eta_{obc} \tag{3}$$

at open boundaries. In Eqs. 1–3, $\eta$ and $\mathbf{u} = (u, v)$ denote tidal elevations and zonal and meridional velocity components, respectively. $H$ is the undisturbed water depth; $g$, $f$, and $a$ are the acceleration due to gravity, the Coriolis parameter, and the Earth radius; and $\kappa$ is the bottom friction parameter. In the subinertial regime (*e.g.*, diurnal tidal constituents in high latitudes), the depth-integrated shallow water equations (Eq. 1) support coastal-trapped topographic wave response to open boundary forcing and, therefore, errors in the Dirichlet conditions can sometimes cause generation of spurious topographic waves near the adjacent coastal boundaries. Radiation OBCs with external sea surface height data (see an overview by Blayo and Debreu 2005) can then be applied at a subset of open ocean boundaries affected by the errors to effectively remove spurious coastal trapped waves. In the super-inertial regime, the dynamical equations do not support coastal-trapped topographic wave response to errors in the Dirichlet OBCs and condition 3 is always sufficient. For example, in an application presented in Section 5 of this paper, both the semidiurnal and diurnal tidal constituents are super-inertial and, therefore, the Dirichlet condition 3 was used exclusively at all open boundaries for all tidal constituents. The bottom friction term in the momentum equations could be specified following any parameterization of modeler's choice. In this work, the bottom friction is specified following a quadratic parameterization and an iterative approximation method. The bottom friction coefficient is

$$\kappa = \frac{C_D|\mathbf{u}_{(0)}|}{H} \tag{4}$$

where $\mathbf{u}_{(0)}$ is the velocity field obtained by running the model with a fixed value of $\kappa$. The nondimensional bottom drag coefficient $C_D$ is a tunable parameter, with values $C_D = 0.002 - 0.003$ typically suggested (*e.g.* Grenier et al. 1995). Note that $\kappa = \kappa(\lambda, \phi)$ is a spatially varying field.

The kinematic and dissipative nonlinearities in the dynamical equations are capable of introducing new frequencies in tidal spectrum through energy transfer from the astronomical tidal constituents to higher and lower frequency harmonics. In this manner, the overtides, compound tides, and low-frequency tides, with frequencies given by the sums and the differences of the astronomical constituent frequencies, can be created. The nonlinear tidal effects can be simulated by introducing the *shallow-water* tidal constituents, which compensate for the nonlinearities and for wave–wave interactions between the astronomical constituents (LeProvost et al. 1981; Andersen et al. 2006). As opposed to the astronomical constituents defined by a unique set of Doodson numbers, the shallow-water constituents have frequencies determined by the multiples of the astronomical constituent frequencies (overtides) or by sums and differences of frequencies of interacting astronomical constituents (compound tides). For example, the nonlinearity in the continuity equation

manifested through the interaction of the $M_2$ and the $S_2$ astronomical constituents gives rise to the $MS_4$ shallow-water constituent. The nonlinear effects generating the shallow-water constituents can be treated within the linearized modeling framework using a perturbation method described in Snyder et al. (1979) and LeProvost et al. (1981). In this manner, the nonlinear effects can be included following a rigorous approach, and a linearized numerical scheme can be formulated for each astronomical or shallow-water constituent.

By searching for solution of Eqs. 1–3 in the form

$$\{\eta, u, v\}(\lambda, \phi, t) = \mathbb{R}\left\{\sum_{k=1}^{K}\left\{\tilde{\eta}_k, \tilde{u}_k, \tilde{v}_k\right\}(\lambda, \phi)\exp\ i\omega_k t\right\}, \tag{5}$$

where $\omega_k$ denotes frequencies of the astronomical and shallow-water tidal constituents and $\tilde{\eta}_k$, $\tilde{u}_k$, and $\tilde{v}_k$ are complex spatially varying fields; we obtain a spectral representation, with a boundary value problem

$$i\omega_k\,\tilde{\eta}_k + \nabla\cdot\begin{bmatrix} H\tilde{u}_k \\ H\tilde{v}_k \end{bmatrix} = 0 \tag{6}$$

$$\begin{bmatrix} \tilde{u}_k \\ \tilde{v}_k \end{bmatrix} = \frac{-g}{(i\omega_k+\kappa)^2 + f^2}\begin{bmatrix} i\omega_k+\kappa & f \\ -f & i\omega_k+\kappa \end{bmatrix}\nabla\tilde{\eta}_k, \tag{7}$$

defined for each individual tidal constituent $k$, subject to the boundary conditions

$$\tilde{\eta}_k\Big|_{\partial\Omega_O} = \zeta_k(x, y) \tag{8}$$

at open boundaries and

$$\mathbf{n}\cdot\begin{bmatrix} \tilde{u}_k \\ \tilde{v}_k \end{bmatrix}\Big|_{\partial\Omega_C} = 0 \tag{9}$$

at closed boundaries. Equations 6–9 can be solved numerically, for example, on an Arakawa-C staggered grid. An outline of the numerical implementation pertinent to the inverse methodology of this paper is discussed next.

## 2.2 Discrete operators and representations

Equations 6–9 discretized on a structured grid lead to a sparse system of equations for a gridded vector $\boldsymbol{\eta}$ of tidal sea surface elevations

$$\mathbf{A}_{\eta\leftarrow\eta}\boldsymbol{\eta} = \mathbf{0}, \tag{10}$$

where matrix $\mathbf{A}_{\eta\leftarrow\eta}$ is a discrete version of the operator

$$\mathcal{A}\{\cdot\} = \left(i\omega_k - \nabla\cdot\frac{gH}{(i\omega_k+\kappa)^2+f^2} \times\begin{bmatrix} i\omega_k+\kappa & f \\ -f & i\omega_k+\kappa \end{bmatrix}\nabla\right). \tag{11}$$

The numerical details of assembling the sparse system matrix $\mathbf{A}_{\eta\leftarrow\eta}$ on an Arakawa-C grid are provided by Logutov and Lermusiaux (2008). In their scheme, $\mathbf{A}_{\eta\leftarrow\eta}$ is nine-diagonal. In the notation followed throughout this paper, the subscripts are utilized to indicate mappings provided by the discrete operators between various staggered grids or variables. For example, the finite-difference operators implementing the gradient differential operator, $g\nabla\{\cdot\}$, utilized in Eq. 7, can be denoted as $\mathbf{G}_{u\leftarrow\eta}$, $\mathbf{G}_{v\leftarrow\eta}$, which indicates that the matrices $\mathbf{G}_{u\leftarrow\eta}$ and $\mathbf{G}_{v\leftarrow\eta}$ act on gridded vectors defined at an $\eta$ grid and provide mappings to $u$ and $v$ Arakawa-C grids, respectively. Similarly, the finite-difference operators implementing the divergence, $(\nabla\cdot)$, can be consistently denoted as $\mathbf{D}_{\eta\leftarrow u}$ and $\mathbf{D}_{\eta\leftarrow v}$ to indicate that the vectors defined at $u$- and $v$-staggered grids constitute the domain of these operators, respectively, while the vectors defined at an $\eta$ grid constitute the range of these operators. Following this notation, the tidal velocity vectors $\mathbf{u}$ and $\mathbf{v}$ are obtained from the tidal elevation vector $\boldsymbol{\eta}$ using Eq. 7

$$\begin{aligned}\mathbf{u} &= \mathbf{U}_{u\leftarrow\eta}\boldsymbol{\eta} \\ \mathbf{v} &= \mathbf{U}_{v\leftarrow\eta}\boldsymbol{\eta},\end{aligned} \tag{12}$$

where the linear operators $\mathbf{U}_{u\leftarrow\eta}$ and $\mathbf{U}_{v\leftarrow\eta}$ are sparse matrices, assembled following a finite-difference scheme of modeler's choice for the gradient and the matrix multiplication acting on the gradient of tidal elevations, $\tilde{\eta}_k$, in Eq. 7.

Further, let vector $\boldsymbol{\zeta} \in \mathbb{C}^{n_\zeta}$ denote a control space of a tidal model, that is, the partition of the state-space and/or tunable parameters that we would like to utilize to steer the model fields towards observations as part of data assimilation procedures. The exact composition of the control space $\boldsymbol{\zeta}$ might vary across different tidal modeling systems and applications. For example, the control space might include the OBCs. Alternatively, a parameterized increment to model bathymetry or bottom friction parameters can be utilized, among other options. To provide a level of generality, we leave the choice of the control space to the discretion of the modeler and only require that a model can be linearized with respect to the control parameters for the purposes of data assimilation. This latter requirement amounts to

an assumption that the control space is separable from the state-space following

$$\mathbf{A}_{(\mathbf{x}\leftarrow\mathbf{x})}\mathbf{x} = \mathbf{B}_{(\mathbf{x}\leftarrow\zeta)}\boldsymbol{\zeta}, \tag{13}$$

where $\mathbf{x} \in \mathbb{N}^{n_\mathbf{x}}$ is the model state-space. In order to provide a specific example of how Eq. 13 is obtained, suppose that the OBCs are chosen as the control space. The sea surface elevation vector $\boldsymbol{\eta} \in \mathbb{C}^N$ in Eq. 10 contains active, masked, and open boundary grid-nodes. Let the indices of active and open boundary $\eta$-points be denoted as $\mathbf{i}_\mathbf{x} \in \mathbb{N}^{n_\mathbf{x}}$ and $\mathbf{i}_\zeta \in \mathbb{N}^{n_\zeta}$, respectively, following the index notation in the Appendix. We can separate the partitions of the system matrix $\mathbf{A}_{\eta\leftarrow\eta}$ corresponding to active and open boundary nodes as

$$\mathbf{A}_{(\mathbf{x}\leftarrow\mathbf{x})} \equiv \left(\mathbf{A}_{\eta\leftarrow\eta}\right)_{\mathbf{i}_\mathbf{x},\mathbf{i}_\mathbf{x}}, \qquad \mathbf{A}_{(\mathbf{x}\leftarrow\boldsymbol{\eta}_\zeta)} \equiv \left(\mathbf{A}_{\eta\leftarrow\eta}\right)_{\mathbf{i}_\mathbf{x},\mathbf{i}_\zeta}. \tag{14}$$

In the foregoing, the index notation in the Appendix is followed. With these partitions, the computational discretization of the dynamical equations (Eq. 10) at active grid-points is given by

$$\mathbf{A}_{(\mathbf{x}\leftarrow\mathbf{x})}\mathbf{x} = -\mathbf{A}_{(\mathbf{x}\leftarrow\zeta)}\boldsymbol{\zeta} \tag{15}$$

where vector $\boldsymbol{\zeta}$ contains the values of the OBCs. The right-hand side in Eq. 15 represents ocean open boundary forcing and the overall system is a specific form of Eq. 13, with the OBCs providing the control space. Alternatively, the bottom friction parameters can be added to the control space. With such a choice, Eq. 7 needs to be linearized with respect to $\kappa(\lambda, \phi)$ and the first variation of the dynamical equations with respect to $\kappa$ needs to be included in the right-hand side of Eq. 13. By seeking to control the model through a chosen set of the control parameters, the inverse solution is fitted to regional observations in accord with the dynamics. After assimilation, the interior and the boundary inverse tidal fields satisfy the barotropic shallow water dynamical equations exactly.

System 13 provides the dynamical constraints for the inverse method. At high resolution, Eq. 13 is solved using iterative methods. We use the preconditioned conjugate gradient method, with the left and the right preconditioners obtained by computing an incomplete LU decomposition of $\mathbf{A}_{(\mathbf{x}\leftarrow\mathbf{x})}$. Such preconditioning leads to an acceleration of convergence of the method and allows for a state-space with a dimensionality of up to $\mathcal{O}(10^6)$. The solution of Eq. 13 will hereby be *formally* denoted as

$$\mathbf{x} = \mathbf{M}_{(\mathbf{x}\leftarrow\zeta)}\boldsymbol{\zeta}, \tag{16}$$

where

$$\mathbf{M}_{(\mathbf{x}\leftarrow\zeta)} = \mathbf{A}^{-1}_{(\mathbf{x}\leftarrow\mathbf{x})}\mathbf{B}_{(\mathbf{x}\leftarrow\zeta)}. \tag{17}$$

In practice, the inverse $\mathbf{A}^{-1}_{(\mathbf{x}\leftarrow\mathbf{x})}$ is never formed explicitly. Equation 17 merely represents an iterative solution of a linear system $\mathbf{A}_{(\mathbf{x}\leftarrow\mathbf{x})}\mathbf{X} = \mathbf{Y}$ for the unknowns $\mathbf{X} \in \mathbb{C}^{n_\mathbf{x}\times p}$ and the right-hand side $\mathbf{Y} = \mathbf{B}_{(\mathbf{x}\leftarrow\zeta)}\mathbf{Z}_\zeta$, ($\mathbf{Z}_\zeta \in \mathbb{C}^{n_\zeta\times p}$).

## 3 Methodology

### 3.1 Setup and logistics

The methodology presented in this paper is designed to employ nested domains around coastal segments where tidal observations are collected but model resolution is insufficient to fully resolve the tidal dynamics. The outer model domain will be referred to as the *control* domain throughout this paper, consistent with the definition of the control parameters in that domain. The variables and the parameters defined in the control domain are labeled throughout using the subscript 0. The nested model domains are setup within the control domain and, without loss of generality, are assumed to be nonoverlapping. To maintain generality, it is assumed that there are $m$ nested domains. The variables and the parameters defined in the nested domains will be labeled throughout using the subscripts $i \in \{1, 2, \ldots, m\}$. Figure 1 presents a schematic of the

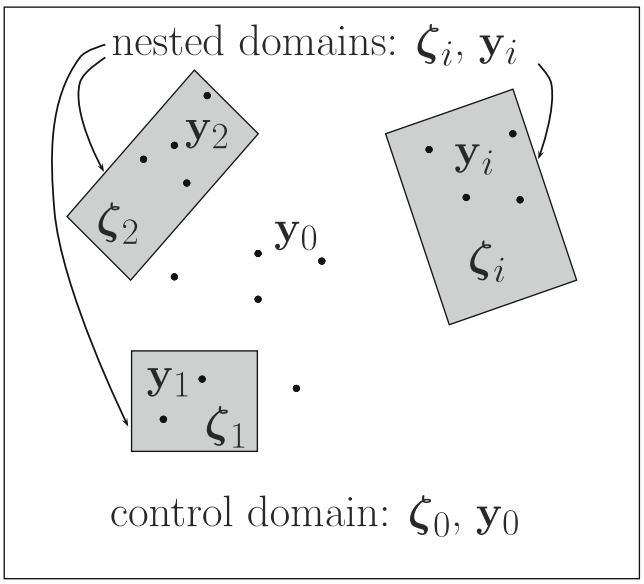


**Fig. 1** Schematic of the control and nested domains. The data assimilation scheme tunes the control parameters $\boldsymbol{\zeta}_0$, defined in the control domain, based on the observational data $\mathbf{y}_0$, $\mathbf{y}_1, \mathbf{y}_2, \ldots, \mathbf{y}_m$. The data-model misfits for $\mathbf{y}_i, i \in \{1, 2, \ldots, m\}$, are obtained based on the nested model computations. A nested domain $i$ is coupled to the outer domain via the OBCs, $\boldsymbol{\zeta}_i$

control and the nested domains and the observations. The control space $\boldsymbol{\zeta}$ is defined in the outer domain and, therefore, will be denoted as $\boldsymbol{\zeta}_0$. The nested domains are coupled to the control domain through the OBCs, $\boldsymbol{\zeta}_i, i \in \{1, 2, \ldots, m\}$. In the forward problem, the control domain provides the OBCs for the nested domains but the computations in the nested domains do not affect the computation in the control domain. In the inverse problem, the computations in the nested domains affect the solution in the control domain through adjustments made to $\boldsymbol{\zeta}_0$ based on the data-nested model misfits. The goal of this section is to provide an optimal scheme for tuning the control parameters, $\boldsymbol{\zeta}_0$, based on the observation-minus-forecast residuals in the outer and the nested domains.

### 3.2 Observational data

Tidal observations may come in the form of sea surface height (SSH) and velocity measurements. Such measurements are obtained from a variety of instruments and platforms, such as moorings, coastal tide gauges, bottom mounted tide gauges, and satellite altimetry, among others. The spectral modeling framework described in Section 2 assumes that the observations are harmonically analyzed and converted to harmonic amplitudes $\{\tilde{\eta}_k, \tilde{u}_k, \tilde{v}_k\}$ for each individual tidal constituent. Details of such a conversion are provided in Logutov and Lermusiaux (2008). The spectral domain data are related to the time domain variables via Eq. 5. Let vectors $\boldsymbol{\eta}_{obs} \in \mathbb{C}^{n^{\eta}_{obs}}$, $\boldsymbol{u}_{obs} \in \mathbb{C}^{n^{u}_{obs}}$, and $\boldsymbol{v}_{obs} \in \mathbb{C}^{n^{v}_{obs}}$ denote the observed values of the tidal elevations $\tilde{\eta}_k$ and the zonal and meridional barotropic tidal velocities $\tilde{u}_k$ and $\tilde{v}_k$ at observation locations. The total observational vector $\mathbf{y} \in \mathbb{C}^{n_{obs}}$ obtained by concatenation

$$\mathbf{y} = \begin{bmatrix} \boldsymbol{\eta}_{obs} \\ \boldsymbol{u}_{obs} \\ \boldsymbol{v}_{obs} \end{bmatrix}_{n_{obs}} \tag{18}$$

is collected throughout the control domain including the areas covered and not covered by the nested domains, as illustrated in the schematic in Fig. 1. The nested domains are setup at a high resolution sufficient to ensure that the collected measurements are representative of the tidal dynamics of the nested models. By permutating the order of entries in $\mathbf{y}$, we hereby introduce the partitions of the observational data, $\mathbf{y} = \{\mathbf{y}_0, \mathbf{y}_1, \ldots, \mathbf{y}_m\}$, based on their location with respect to the nested domains. The observational data inside the $i$th nested domain is denoted as $\mathbf{y}_i$, while the observational data inside the control domain but outside of any of the nested domains is denoted as $\mathbf{y}_0$ (Fig. 1)

$$\mathbf{y} = \begin{bmatrix} \mathbf{y}_0 \\ \mathbf{y}_1 \\ \vdots \\ \mathbf{y}_m \end{bmatrix}_{n_{obs}}, \tag{19}$$

with the ordering of the SSH and the velocity measurements in each $\mathbf{y}_i$ given in Eq. 18. Errors associated with measurements can typically be assumed independent between observation locations leading to a diagonal observational error covariance model. We will here assume only that the observational error covariance has a block-diagonal structure, with the measurement error uncorrelated across the domains

$$\mathbf{R} \equiv \mathcal{E}\left\{\boldsymbol{\epsilon}_{\mathbf{y}} \boldsymbol{\epsilon}_{\mathbf{y}}^{H}\right\} = \begin{bmatrix} \mathbf{R}_0 & & & \\ & \mathbf{R}_1 & & \\ & & \ddots & \\ & & & \mathbf{R}_m \end{bmatrix}_{n_{obs} \times n_{obs}}. \tag{20}$$

Each block $\mathbf{R}_i$ can be specified based on any practical considerations with respect to measurement error in each domain or estimated using the methods of error covariance parameter estimation from data-model misfits (*e.g.*, Dee 1995). Finally, let $\mathbf{H}_{\mathbf{y}_i \leftarrow \mathbf{x}_i}$ denote an observational operator relating the model state-space, $\mathbf{x}_i$, in the $i$th model domain to the observation vector in that domain. In its simplest form, an observational operator represents an interpolation from a model grid onto the observation locations. For the velocity measurements, an observational operator includes the linear mappings $\mathbf{U}_{u \leftarrow \eta}$ and $\mathbf{U}_{v \leftarrow \eta}$ defined in Eq. 12, in addition to interpolation. Following the notation, data-model misfits corresponding to a tidal solution obtained in each model domain are given by

$$\mathbf{d}_i = \mathbf{y}_i - \mathbf{H}_{\mathbf{y}_i \leftarrow \mathbf{x}_i} \mathbf{x}_i, \tag{21}$$

where $\mathbf{x}_i$ denotes the model state-space in the $i$th model domain, with the control domain counted as the 0th model domain.

### 3.3 Forward model error covariance

The control parameters $\boldsymbol{\zeta}_0$ can be assigned some a priori values. For example, the a priori values of the OBCs can be specified from a global tidal model. Let $\hat{\boldsymbol{\zeta}}_0$ denote the a priori values of the control parameters, with the corresponding error covariance $\mathbf{P}_0$. Theoretical statements about the sources of error in $\hat{\boldsymbol{\zeta}}_0$ combined with practical considerations lead to a specific

form of $\mathbf{P}_0$. In practice, $\mathbf{P}_0$ is not well known and merely reflects the degree of accuracy that a modeler associates with the a priori estimate $\hat{\boldsymbol{\zeta}}_0$. Given the lack of objective information about $\mathbf{P}_0$, it can be sufficiently expressed using a low-rank approximation

$$\mathbf{P}_0 = \mathbf{Z}_0 \mathbf{Z}_0^H, \tag{22}$$

with $\mathbf{Z}_0 \in \mathbb{C}^{n_\zeta \times p}$ containing $p$ dominant orthogonal control parameter error subspaces. The error subspaces $\mathbf{Z}_0$ can be obtained, for example, via a singular value decomposition (svd) of a valid parametric covariance form $\mathbf{G}_0$,

$$\mathbf{G}_0 = \mathbf{U}_0 \boldsymbol{\Lambda}_0 \mathbf{U}_0^T, \qquad \mathbf{Z}_0 \equiv \mathbf{U}_0 \boldsymbol{\Lambda}_0^{1/2}, \tag{23}$$

*e.g.* an svd of a Gaussian parametric form given in Eq. 39. Alternatively, $\mathbf{Z}_0$ can be specified via the Gramm–Schmidt orthogonalization of an ensemble of the control parameters. The number, $p$, of orthogonal error subspaces retained in $\mathbf{P}_0$ is at the discretion of the modeler and can be adjusted as needed. It will be shown below that the orthogonal matrix $\mathbf{Z}_0$ provides a linear basis for an analysis increment of the control parameters. Therefore, rank $p$ should be chosen such as to ensure that $\mathbf{Z}_0$ provides a sufficient linear basis depending on a specific application. With the OBCs utilized as the control space, the a priori values $\hat{\boldsymbol{\zeta}}_0$ can be specified from a global tidal model and $p \leq 100$ is typically sufficient. Following Eq. 16, the model error subspace induced by $\mathbf{Z}_0$ is given by

$$\mathbf{Z}_{\mathbf{x}_0} = \mathbf{M}_{(\mathbf{x}_0 \leftarrow \boldsymbol{\zeta}_0)} \mathbf{Z}_0. \tag{24}$$

As before, the operator $\mathbf{M}_{(\mathbf{x}_0 \leftarrow \boldsymbol{\zeta}_0)}$ represents an iterative solution of Eq. 13, with the right-hand side given by $\mathbf{B}_{(\mathbf{x}_0 \leftarrow \boldsymbol{\zeta}_0)} \mathbf{Z}_0$. Equation 24 can be solved efficiently even for large $(10^3 - 10^4)$ values of $p$ by, firstly, carrying out an incomplete LU factorization of $\mathbf{A}_{(\mathbf{x} \leftarrow \mathbf{x})}$ with small values of drop tolerance and, secondly, using the computed LU factors as preconditioners of the conjugate gradient solver. $\mathbf{Z}_{\mathbf{x}_0} \in \mathbb{C}^{n_\mathbf{x} \times p}$ is the matrix square root of the forward model error covariance

$$\mathbf{P}_{\mathbf{x}_0} = \mathbf{Z}_{\mathbf{x}_0} \mathbf{Z}_{\mathbf{x}_0}^H, \tag{25}$$

induced by the control parameter error propagated from the control space to the model state-space in the control domain. The formalism can be further applied to obtain the matrix square roots of forward model error covariances in the nested domains, in addition to the control domain. The nested domains are coupled to the control domain through the OBCs, $\boldsymbol{\zeta}_i$. With $\mathbf{H}_{\boldsymbol{\zeta}_i \leftarrow \mathbf{x}_0}$ denoting an interpolation from the state-space in the control domain onto the open boundaries of the $i$th nested domain

$$\boldsymbol{\zeta}_i = \mathbf{H}_{\boldsymbol{\zeta}_i \leftarrow \mathbf{x}_0} \mathbf{x}_0, \tag{26}$$

the square root of the OBC error covariance in the $i$th nested domain is given by

$$\mathbf{Z}_i = \mathbf{H}_{\boldsymbol{\zeta}_i \leftarrow \mathbf{x}_0} \mathbf{Z}_{\mathbf{x}_0}. \tag{27}$$

The subspaces $\mathbf{Z}_i$, can, next, be propagated through the corresponding nested tidal models, similarly to Eq. 24,

$$\mathbf{Z}_{\mathbf{x}_i} = \mathbf{M}_{(\mathbf{x}_i \leftarrow \boldsymbol{\zeta}_i)} \mathbf{Z}_i. \tag{28}$$

Equation 28 represents an uncertainty propagation from the OBC space of the nested domains to the state-space of the nested domains. As in Eq. 16, operator $\mathbf{M}_{(\mathbf{x}_i \leftarrow \boldsymbol{\zeta}_i)}$ is a formal representation of the numerical procedures solving the dynamical equations in the nested domains, with the open boundary forcing provided by $\mathbf{Z}_i$. Solution of the dynamical equations (Eq. 28) yields the square roots of the forward model error covariances in the nested domains. In conjunction with Eqs. 24 and 27, the procedure amounts to propagating an uncertainty from the control space $\boldsymbol{\zeta}_0$ to the state-spaces of the nested tidal models.

### 3.4 Estimation of control parameters

An optimization problem is posed using a quadratic cost functional penalizing the (weighted) variance of the observation-minus-forecast residuals in the control and the nested domains

$$\hat{\boldsymbol{\zeta}}_* = \arg\min_{\boldsymbol{\zeta}} J(\boldsymbol{\zeta}), \tag{29}$$

$$J(\boldsymbol{\zeta}) = (\boldsymbol{\zeta} - \hat{\boldsymbol{\zeta}}_0)^H \mathbf{P}_0^{-1} (\boldsymbol{\zeta} - \hat{\boldsymbol{\zeta}}_0) + \sum_{i=0}^{m} \left(\mathbf{y}_i - \mathbf{H}_{\mathbf{y}_i \leftarrow \mathbf{x}_i} \mathbf{x}_i\right)^H \mathbf{R}_i^{-1} \left(\mathbf{y}_i - \mathbf{H}_{\mathbf{y}_i \leftarrow \mathbf{x}_i} \mathbf{x}_i\right).$$

In Bayesian interpretation, the first term in Eq. 29 represents the prior information about the control parameters. It can also be viewed as a regularization term added to penalize a deviation of the control parameter values from their a priori values. The definition (Eq. 29) of a penalty functional is equivalent to the minimum error variance estimation in the control parameter space (Logutov 2007). The minimization problem (Eq. 29) is subject to the linear constraints

$$\mathbf{x}_i = \mathbf{M}_{(\mathbf{x}_i \leftarrow \boldsymbol{\zeta}_i)} \boldsymbol{\zeta}_i, \qquad \forall i \in \{0, 1, \ldots, m\}, \tag{30}$$

with $\mathbf{M}_{(\mathbf{x}_i \leftarrow \zeta_i)}$ described in Eq. 17 and the OBCs $\boldsymbol{\zeta}_i$ obtained via Eq. 26. Equations 29–30 fall into a general class of quadratic minimization problems with linear constraints.

To provide a practical method of solution of Eqs. 29–30, we, first, establish the notation that unifies the linear constraints (Eq. 30). By combining Eqs. 30 and 26, a nested state-space, $\mathbf{x}_i$, is related to the control parameters via

$$\mathbf{x}_i = \mathbf{M}_{(\mathbf{x}_i \leftarrow \zeta_0)} \boldsymbol{\zeta}_0 \tag{31}$$

with the operator $\mathbf{M}_{(\mathbf{x}_i \leftarrow \zeta_0)}$ given by

$$\mathbf{M}_{(\mathbf{x}_i \leftarrow \zeta_0)} \equiv \mathbf{M}_{(\mathbf{x}_i \leftarrow \zeta_i)} \mathbf{H}_{\zeta_i \leftarrow \mathbf{x}_0} \mathbf{M}_{(\mathbf{x}_0 \leftarrow \zeta_0)}. \tag{32}$$

Consistently with the notation, the operator $\mathbf{M}_{(\mathbf{x}_i \leftarrow \zeta_0)}$ is a formal representation of the following numerical procedures: solution of the dynamical equations in the outer domain, interpolation of the solution to open boundaries of the *i*th nested domain, followed by a solution of the dynamical equations in the *i*th nested domain. Finally, let

$$\mathbf{M}_{(\mathbf{y} \leftarrow \zeta_0)} \equiv \begin{bmatrix} \mathbf{H}_{\mathbf{y}_0 \leftarrow \mathbf{x}_0} \mathbf{M}_{(\mathbf{x}_0 \leftarrow \zeta_0)} \\ \mathbf{H}_{\mathbf{y}_1 \leftarrow \mathbf{x}_1} \mathbf{M}_{(\mathbf{x}_1 \leftarrow \zeta_0)} \\ \cdots \\ \mathbf{H}_{\mathbf{y}_m \leftarrow \mathbf{x}_m} \mathbf{M}_{(\mathbf{x}_m \leftarrow \zeta_0)} \end{bmatrix} \tag{33}$$

denote the total dynamical operator providing the multigrid model values of the tidal fields at observation locations given the values of the control parameters. The observational operators $\mathbf{H}_{\mathbf{y}_i \leftarrow \mathbf{x}_i}$ are described in the text leading to Eq. 21. The linear dynamical constraints are now unified through $\mathbf{M}_{(\mathbf{y} \leftarrow \zeta_0)}$. With these dynamical constraints substituted directly into Eq. 29, the penalty functional is expressed

$$\begin{aligned} J(\boldsymbol{\zeta}_0) = {} & (\boldsymbol{\zeta}_0 - \hat{\boldsymbol{\zeta}}_0)^H \mathbf{P}_0^{-1} (\boldsymbol{\zeta}_0 - \hat{\boldsymbol{\zeta}}_0) \\ & + \left(\mathbf{y} - \mathbf{M}_{(\mathbf{y} \leftarrow \zeta_0)} \boldsymbol{\zeta}_0\right)^H \mathbf{R}^{-1} \left(\mathbf{y} - \mathbf{M}_{(\mathbf{y} \leftarrow \zeta_0)} \boldsymbol{\zeta}_0\right), \end{aligned} \tag{34}$$

with the block-diagonal $\mathbf{R}$ given in Eq. 20. The quadratic functional Eq. 34 is convex and has a unique minimum. The solution can be derived in closed form by expressing the first variation of Eq. 34 with respect to the control parameters $\boldsymbol{\zeta}$ and setting it to zero. The minimum is reached at

$$\begin{aligned} \hat{\boldsymbol{\zeta}}_* = {} & \hat{\boldsymbol{\zeta}}_0 + \mathbf{P}_0 \mathbf{M}^H_{(\mathbf{y} \leftarrow \zeta_0)} \left(\mathbf{M}_{(\mathbf{y} \leftarrow \zeta_0)} \mathbf{P}_0 \mathbf{M}^H_{(\mathbf{y} \leftarrow \zeta_0)} + \mathbf{R}\right)^{-1} \\ & \times \left(\mathbf{y} - \mathbf{M}_{(\mathbf{y} \leftarrow \zeta_0)} \hat{\boldsymbol{\zeta}}_0\right). \end{aligned} \tag{35}$$

With the a priori error covariance $\mathbf{P}_0$ provided by Eq. 22, the analysis equation (Eq. 35) can be equivalently expressed as

$$\hat{\boldsymbol{\zeta}}_* = \hat{\boldsymbol{\zeta}}_0 + \mathbf{Z}_0 \boldsymbol{\beta}. \tag{36}$$

As was eluded to in Section 3.3, the orthogonal matrix $\mathbf{Z}_0$ provides a linear basis for an analysis increment of the control parameters. Complex coefficients $\boldsymbol{\beta} \in \mathbb{C}^p$ are obtained from the observation-minus-forward model residuals

$$\boldsymbol{\beta} = \tilde{\mathbf{Z}}^H \left(\tilde{\mathbf{Z}} \tilde{\mathbf{Z}}^H + \mathbf{R}\right)^{-1} \left(\mathbf{y} - \mathbf{M}_{(\mathbf{y} \leftarrow \zeta_0)} \hat{\boldsymbol{\zeta}}_0\right) \tag{37}$$

$$\tilde{\mathbf{Z}} = \mathbf{M}_{(\mathbf{y} \leftarrow \zeta_0)} \mathbf{Z}_0. \tag{38}$$

Matrix $\tilde{\mathbf{Z}}$ is the square root of the error covariance propagated from the control parameter space to observation locations through a tidal dynamical model in the multigrid settings. Analysis equations (Eqs. 36–38) provide a practical method of data assimilation using multigrid resolving computations. The steps of the inverse solution are summarized below.

### 3.5 Summary of the inverse solution

First, a choice of the square root matrix $\mathbf{Z}_0$ is made, for example, by following Eq. 23 or via the Gramm–Schmidt orthogonalization of an ensemble of the control parameters. Numerical solution of the dynamical equations (Eq. 13) is, next, carried out in the outer domain, with forcing provided by $\mathbf{B}_{(\mathbf{x} \leftarrow \zeta)} \mathbf{Z}_0$. The result, the square-root $\mathbf{Z}_{\mathbf{x}_0}$, is interpolated onto the open boundaries of the nested domains to provide the OBCs for the nested computations. The dynamical equations in the nested domains are subsequently solved and the square-roots $\mathbf{Z}_{\mathbf{x}_i}$ are generated. Finally, the observational operators $\mathbf{H}_{\mathbf{y}_i \leftarrow \mathbf{x}_i}$ are applied to $\mathbf{Z}_{\mathbf{x}_i}$ in each domain and the square-root $\tilde{\mathbf{Z}}$ in Eq. 38 is obtained. The analysis increment in the control space is computed via Eqs. 36–38, and the multigrid tidal modeling system is run again, with the analysis values of the control parameters, to yield the inverse tidal solution in the control and in the nested domains.

## 4 Discussion

The key point of divergence of various data assimilation schemes is the method by which an uncertainty is estimated and propagated through a dynamical model (Lermusiaux et al. 2006a). Adjoint methods seek to optimize a model state-space trajectory with respect to measurements and the a priori boundary and initial conditions by solving the coupled forward and adjoint dynamical equations arising from the principles of calculus of variations (Bennett 1992). The

representer method refers to a specific way of solving the coupled forward/adjoint systems by their decoupling of each other, suitable for linearized dynamical systems (Egbert et al. 1994). In these methods, various sources of uncertainty are accounted for by specifying the error covariances or convolution kernels affecting the forcing terms of the forward dynamical system. In contrast, the KF based assimilation algorithms evolve an uncertainty in the model state-space by integrating the linearized error covariance evolution equations, potentially embedded in the stochastic environment (Heemink and Kloosterhuis 1990). Stochastic primitive equation ocean models propagate and model an uncertainty by adding random perturbations, with specified characteristics, to a deterministic primitive equation ocean model to represent the effect of various error sources (Lermusiaux 2006). In the method presented in this paper, data assimilation is carried out, with the mediation of nested computation(s), by propagating an uncertainty from a control space in the outer domain to model tidal fields at observation locations in the outer and in the nested domains using low-rank error covariance representations (Lermusiaux and Robinson 1999). An analysis increment in the control space is computed by minimizing the (weighted) variance of the observation-minus-forecast residuals constructed using nested resolving computations.

The methodology relies on steering the model state-space towards observations by adjusting the values of the parameters in a chosen control space. Because an assimilation scheme is implemented by means of a chosen set of the control parameters, the inverse tidal fields are in a perfect dynamical balance, uniform across the multigrid system. The specific choice of the model control space is left to the discretion of the modeler and depends on a specific application. A level of generality was intentionally retained throughout this presentation with respect to the choice of the control space. The only requirement imposed was that the model dynamics can be linearized with respect to the control parameters for the purposes of data assimilation. As an example, the OBCs provide a sensible control space in regional tidal modeling applications (Logutov and Lermusiaux 2008). In coastal waters, the tidal forcing occurs mainly through the OBCs and constitutes a significant source of uncertainty. The OBCs of regional tidal models are typically prescribed from global tidal estimates, for example, from TPXO (Egbert and Erofeeva 2002) or FES95 (LeProvost et al. 1994) global models. The resolution of global models is insufficient to fully resolve regional topographic and coastal features, and, therefore, tuning the OBCs consistently with the regional tidal dynamics and the measurements is sensible. The choice of the OBCs as the control space is adopted for the illustration of the method in the next section. Alternatively, the bottom friction parameters or bottom topography parameters can be utilized as the control space. Linearization of the dynamical equations with respect to the OBCs is straightforward, presented in Section 2. Linearization with respect to the bottom friction parameters is also feasible, briefly described in Section 2 but not followed upon. The next section provides a real-world example of an application of the described methodology in the context of the PhilEx.

## 5 PhilEx case study

The PhilEx project, an ongoing effort at the time of this writing, was designed as a multi-institutional, wide-range study of spatial and temporal variability of the oceanographic processes in and around the straits of the Philippine Archipelago, with an overall goal of better understanding the archipelago dynamics and improving the capability to model and predict regional and coastal ocean processes in areas with diverse topographic conditions. A wide variety of topographic conditions, including enclosed and semienclosed seas connected through a network of channels and sills, make tidal modeling in the waters of the Philippines an exceptionally challenging task. The logistics of the modeling component of PhilEx required that the tidal computations were carried out in a domain covering the Philippines Archipelago, as well as portions of the Pacific and Indian oceans shown in Fig. 2. Computational constraints and other considerations led us to use a structured grid spectral barotropic tidal model (Logutov and Lermusiaux 2008) at a 5-min resolution for that domain. The 5-min resolution domain will be referred to hereafter as the *control* or *outer* domain, consistently with the previous notation. The bottom topography was specified from 1-min resolution (Smith and Sandwell 1997) (version 9.1) bathymetry data set, the highest resolution bathymetry product available to us. Appropriate smoothing was applied to the bathymetric data to avoid aliasing when specifying the model grid at 5-min resolution. The a priori values of the OBCs were obtained from the 1/4-degree resolution TPXO7.0 global tidal model (Egbert and Erofeeva 2002).

Tidal observations available to us consisted of the Topex-Poseidon (TP) satellite altimeter data, with tracks shown in Fig. 2, and the velocity and the SSH data from two moorings in the Panay (A1) and the Dipolog (A2) straits. The A1 and A2 moorings were

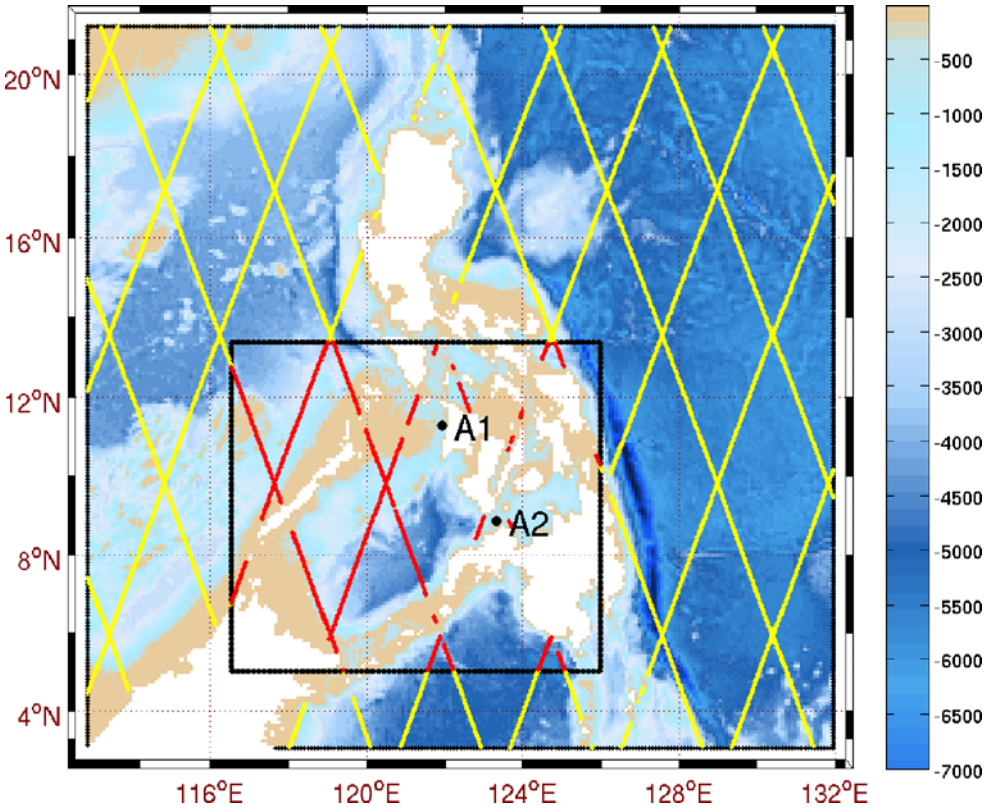


**Fig. 2** Bathymetry [m] in PhilEx 5-min resolution model domain and the observational data. The *black bounding box* shows the nested 1-min resolution domain. The observational network consisted of the Topex/Poseidon altimetry and two moorings, *A1* and *A2*. The observational data are partitioned into $\mathbf{y}_0$ (*yellow*) and $\mathbf{y}_1$ (*red*) as explained in text

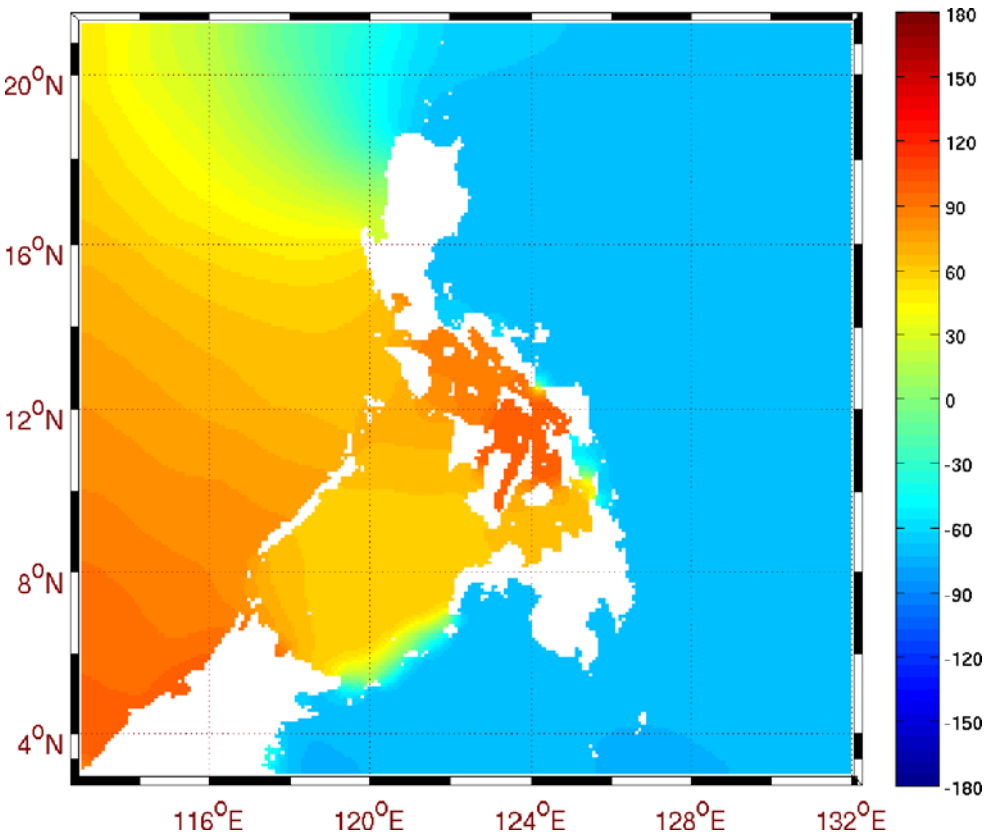


**Fig. 3** $M_2$ Greenwich phase [in deg] based on the forward computations in the outer domain

deployed and operated by the team led by Janet Sprintall of the Scripps Institution of Oceanography as part of PhilEx observational program. In addition to the acoustic doppler current profilers (ADCPs), the moorings were carrying pressure gauges, suitable for inferring the SSH. The TP data, collected from the launch of

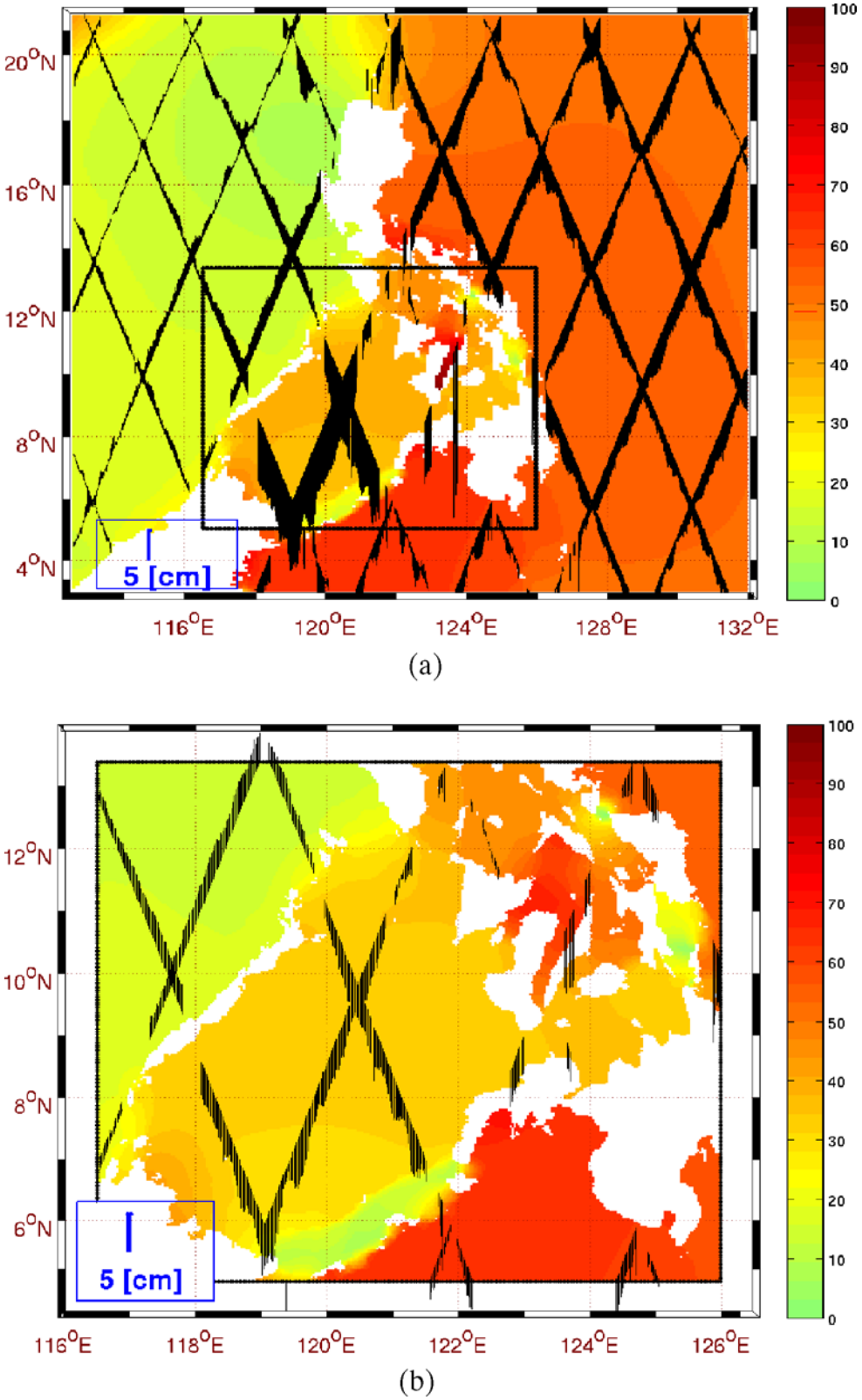


**Fig. 4** Data-forward model misfits for $M_2$. Plotted: SSH amplitude in the control and nested domains. The misfits are plotted as *arrows* originating at TP tracks and pointing up for positive misfits and down for negative. **a** Five-min resolution computation. **b** One-min resolution computation. Arrow scale is given in *bottom left corner*

the satellite in 1992, were provided to us in the form of tidal constituents (SSH amplitudes and phases) by Dr. Richard Ray of the Planetary Geodynamics Laboratory at the NASA Goddard Space Flight Center (Schrama and Ray 1994; Ray 2001). The TP data were utilized to constrain the model to the observed sea-level elevations; the mooring ADCP and pressure measurements were utilized to validate tidal model outputs. Since the mooring data were utilized for validation, they were not used for assimilation.

Tidal modeling in the Philippine basin is difficult because of the substantial phase and amplitude transitions in tidal constituents across the straits on the eastern boundary of the Archipelago. The transitions occur in the Surigao and the San Bernardino straits connecting the Bohol Sea and the Visayan Sea with the Pacific Ocean, and in the straits of the Sulu Archipelago connecting the Sulu and the Celebes seas. Figure 3 shows the cotidal chart for $M_2$, the dominant tidal constituent in the basin, based on the forward model computations. The $M_2$ tide is out of phase across the Surigao and the San Bernardino straits and has about 100 degrees phase difference across the straits of the Sulu Archipelago. Under these circumstances, the computations are

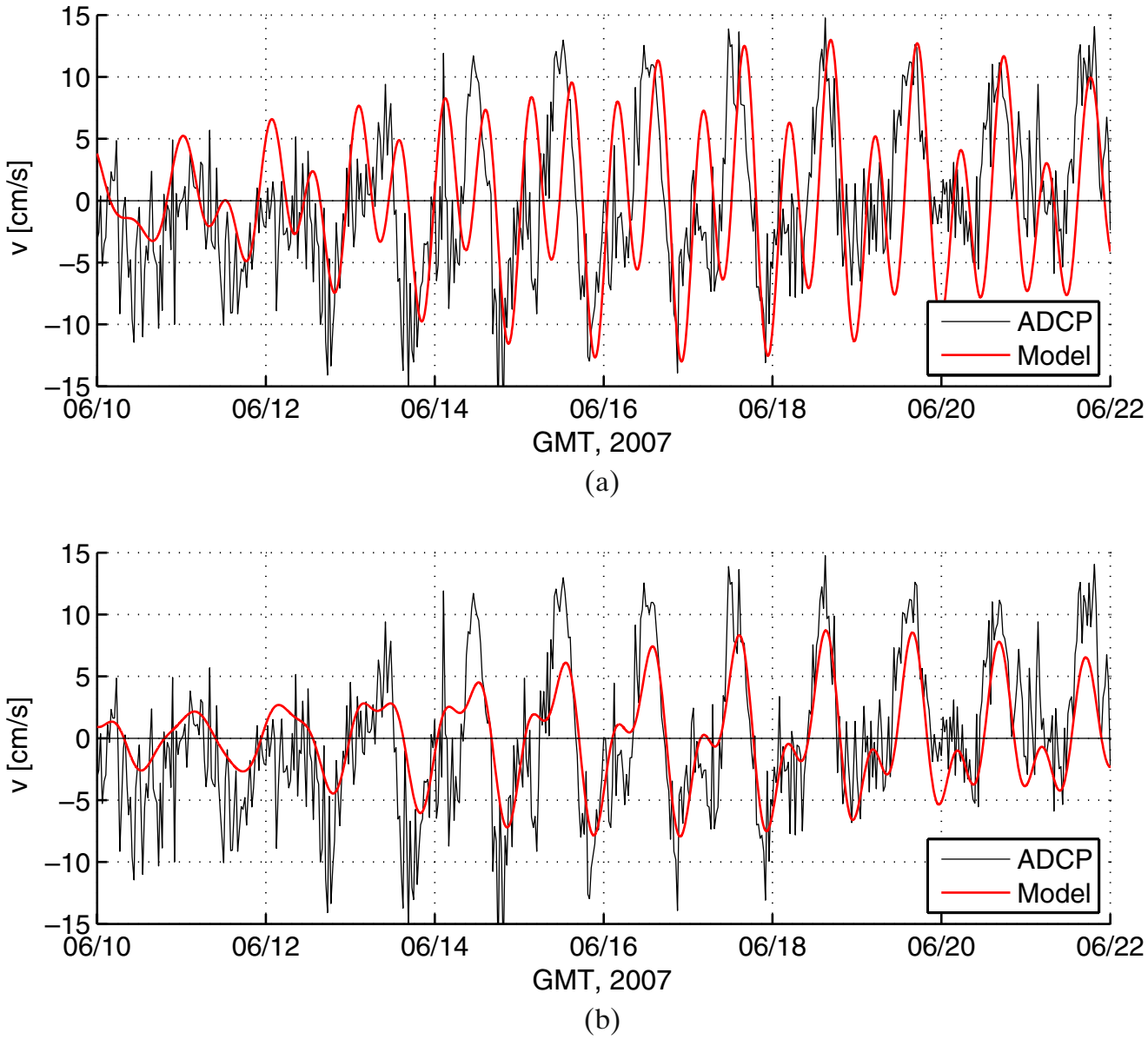


**Fig. 5** Observed and forward model velocity at A1. Observed meridional depth-averaged velocity, with mean removed (*black*). Model velocity (*red*). **a** At 5-min resolution; **b** at 1-min resolution

sensitive to model resolution because the resolution affects the representation of bottom topography and, therefore, tidal transports through the straits. At 5-min resolution, the data-model residuals in the Sulu, Bohol, Visayan, and Sibuyan seas were higher than the average across the model domain. A trial use of a higher-

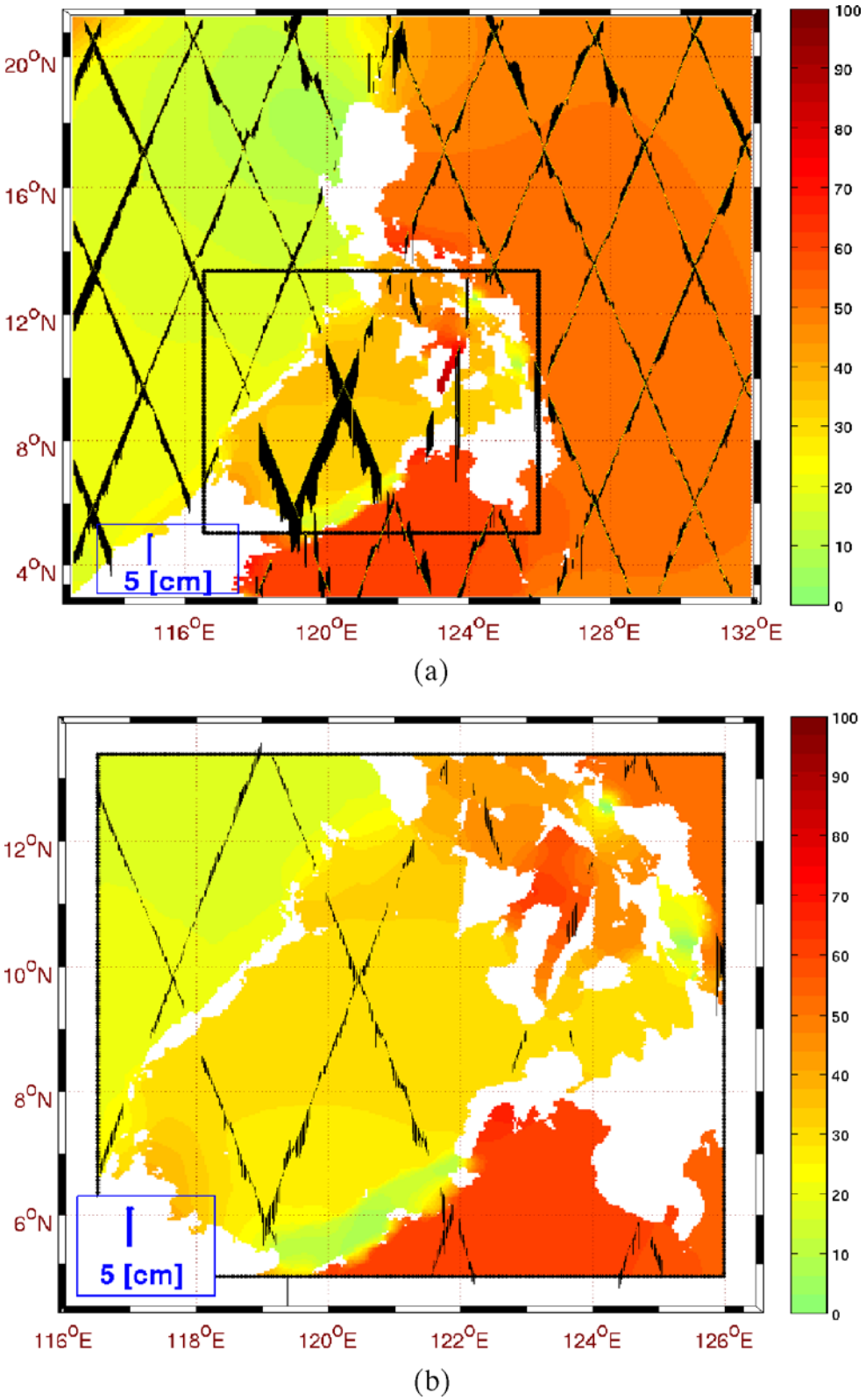


**Fig. 6** Same as Fig. 4 but for the multigrid inverse solution

resolution nested domain covering these basins confirmed that the computations were sensitive to model resolution. Figure 4 shows the SSH amplitudes of the $M_2$ tide modeled at 5-min (panel a) and 1-min (panel b) resolution. Plotted also are the misfits of the observed and the model $M_2$ amplitude. The misfits are plotted as arrows originating at TP tracks and pointing up or down depending on the sign of a misfit, positive, up, and negative, down. Thus, an upward arrow indicates that an observed value is higher than a model value, and vice versa. The misfits are within the 5-cm range at 5-min model resolution, except in the Sulu sea and the adjacent basins. The Sulu, Bohol, Visayan, and Sibuyan seas had model values consistently higher than the observed SSH by an average of 10 cm, with even larger misfits at several locations. The computations at 1-min resolution, however, showed a substantial reduction of data-model misfits. The reduction indicated to us the presence of the representativeness error in these areas. A 1-min resolution domain was, therefore, setup in the Sulu, Bohol, Visayan, and Sibuyan sea basins, shown by the bounding box in Fig. 2, and a task of assimilating the measurements into the 5-min resolution model via the mediation of the nested 1-min resolution domain was presented. The methodology described in this paper allowed us to achieve that task. Figure 5 shows the time series of the observed and the forward model velocity at mooring A1 in the Panay strait. The mooring was located about 3 km off the coast of Panay Island, near a coastal segment with predominantly meridional orientation. The meridional velocity plotted in Fig. 5 corresponds to the along-slope direction. Local bottom topography is a major factor determining a velocity field near coastal moorings. The observation-minus-forecast residuals at A1 were found to be highly sensitive to model resolution. Figure 5 shows the velocities at A1 obtained from the 5-min resolution and the 1-min resolution computations compared against the depth-averaged ADCP velocity measurements. The forward solution in the control domain exhibited significant errors in both amplitude and phase. However, the 1-min resolution nested computations were in closer agreement with the measurements.

To illustrate the utility of our method, the information from the TP data was assimilated into the outer model domain with and without the use of the nested domain. The primary source of tidal forcing in the PhilEx region is provided through the open boundaries. Therefore, the OBCs were chosen as the control space for the purposes of data assimilation. The a priori

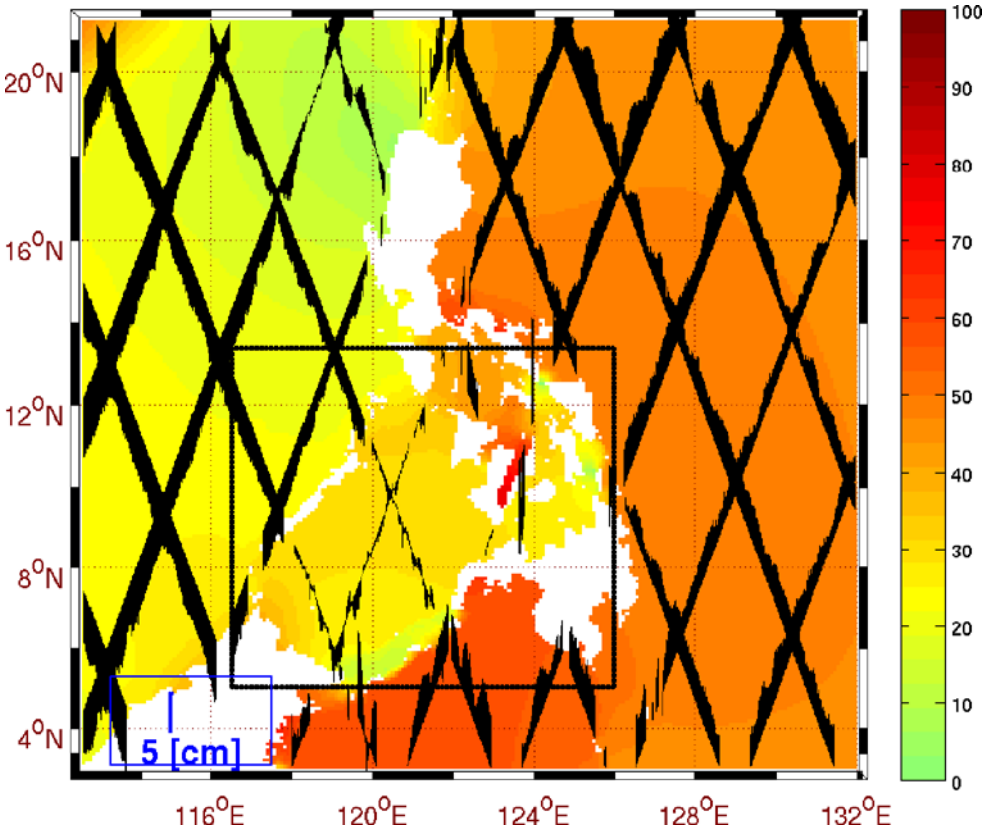


**Fig. 7** Same as Fig. 6a but for the stand-alone inverse computation, with all TP data assimilated directly into the 5-min resolution model

error covariance of the control parameters was specified using a Gaussian two-dimensional parametric form

$$\mathbf{G}_{-}(\mathbf{r},\mathbf{r}_0)=\sigma_0^2\exp\frac{-|\mathbf{r}-\mathbf{r}_0|^2}{2L^2},\quad |(\mathbf{r},\mathbf{r}_0)\in\partial\Omega_O, \tag{39}$$

where $\mathbf{r}$ and $\mathbf{r}_0$ are coordinates of two points on the control domain open boundary. The length scale and the variance parameters in Eq. 39 were chosen $L=100$ km and $\sigma_0^2=(10\,\text{cm})^2$. The svd of Eq. 39, with $p=50$ dominant singular vectors retained, was carried out and Eq. 23 was utilized to obtain $\mathbf{Z}_0$ in Eq. 37. The observations were assumed to have spatially uncorrelated error, with variance $\sigma_o^2=(10\,\text{cm})^2$. Figures 6 and 7 are provided for comparison of the inverse solution for the $M_2$ constituent in the multigrid system and the stand-alone system, respectively. The former shows the SSH amplitude of the multigrid inverse solution, computed using the methodology presented in this paper. The latter presents the amplitude in the stand-alone inverse computation, with all the TP data assimilated directly into the 5-min resolution model. These computations show that fitting the TP data in the Sulu, Bohol, Visayan, and Sibuyan seas directly into the 5-min

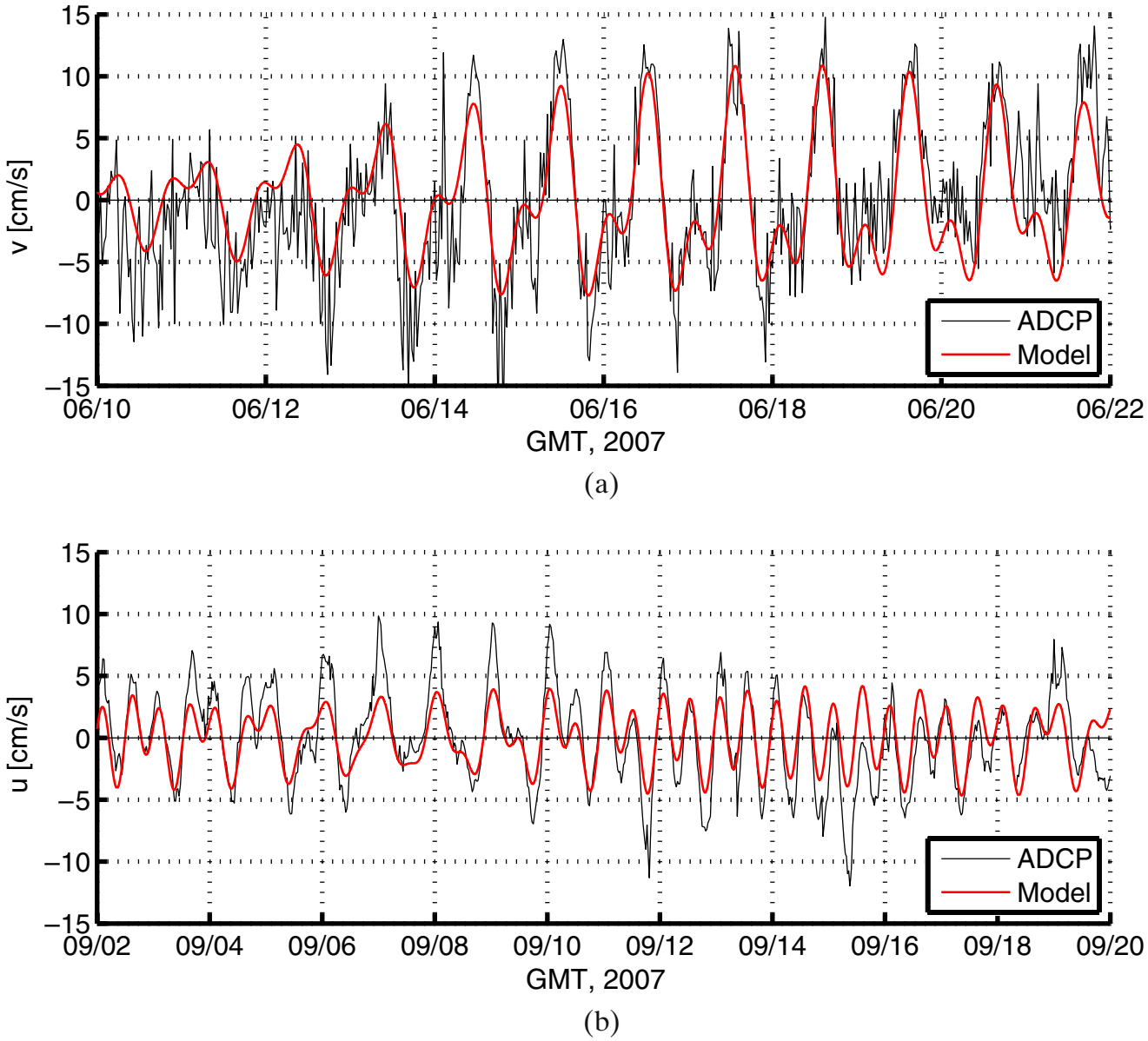


**Fig. 8** Observed vs inverse model velocities at A1 and A2. Plotted are the depth-averaged velocities, with mean removed. **a** Meridional velocity at A1; **b** zonal velocity at A2

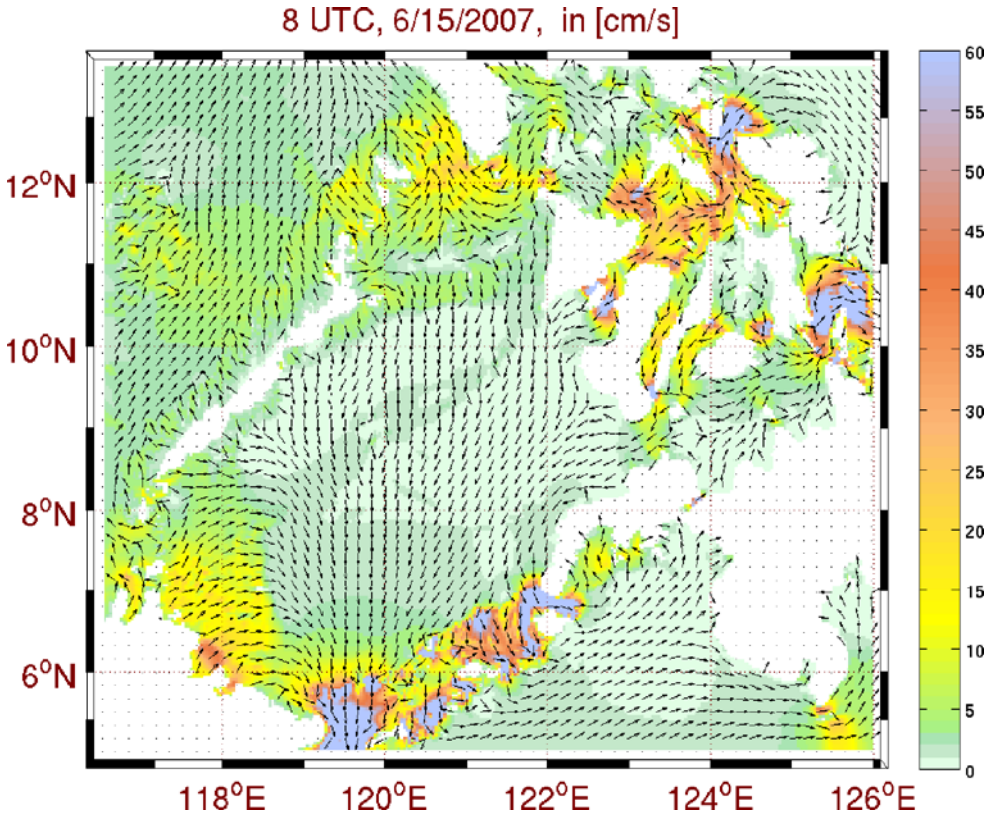


**Fig. 9** Example of a tidal velocity forecast obtained using the inverse scheme. Total tidal velocity valid at 8 UTC, June 15, 2007

resolution model was counter-productive and led to a degradation in the overall model fit to the altimetry. On the contrary, assimilation of the named data subset via the use of the resolving 1-min computation led to a consistent decrease of the overall error. The inverse solution depicted in Fig. 6 provides a fit of the barotropic tidal dynamics to data consistently with the dynamical scales resolved in models and in observations. Figure 8 shows the comparison of the velocity field of the multigrid inverse solution against the ADCP data. An improvement in the velocity field estimates through the use of the multigrid inverse can be analyzed by comparing Figs. 8a and 5b. The match of the ADCP measurements to the inverse model velocity has been substantially improved as compared to the forward model velocity in Fig. 5. On the contrary, the velocity field of the stand-alone inverse solution was in worse agreement (figure not shown) with the ADCP data than the forward solution shown in Fig. 5b. Figure 9 gives an example of the final output of the inverse scheme: the tidal velocity forecast at high resolution, tuned to measurements. The use of the multigrid data-assimilative computations has allowed us to generate reliable barotropic tidal velocity forecasts and demonstrate a good skill in modeling the barotropic tidal circulation despite the challenges presented by the complexity of coastlines and bottom topography.

## 6 Summary and conclusions

The main focus of this paper was a multigrid data-assimilative framework for assimilation of measurements into regional tidal models. A new technique for inverting the observational data in a multigrid setting has been described. The methodology allows to employ nested domains around coastal segments where tidal observations are collected but model resolution is insufficient to fully resolve the tidal dynamics. As was argued in the paper and demonstrated using a real-world application in the context of the PhilEx dynamical experiment, assimilation of measurements inconsistent with the resolved model dynamics can be counter-productive. In regional tidal modeling applications, coastal measurements are often affected by local small-scale coastal and topographic features. For example, the SSH measured in a small bay or in an estuary can have tidal variations substantially different, both in amplitude and in phase, from the nearby open ocean areas, depending on the local characteristics of a coastline and bottom topography. In areas where model resolution is insufficient to resolve the important characteristics of the waterways, the observational data are compounded with the representativeness error. The inverse procedures presented in this paper are designed to suppress the representativeness error by employing

nested resolving computations. This capability is expected to find applications in the context of structured grid regional tidal modeling applications.

The method seeks to assimilate the observational data into a multigrid modeling system by using a set of control parameters chosen at the discretion of the modeler, such as the OBCs. Presently, the control parameters are defined in the outer domain. With this strategy, a model is fitted to data consistently with the dynamics defined uniformly across the entire multigrid computational system. The inverse fields are in a perfect dynamical balance and a transition of the inverse solution across the domain boundaries is seamless and satisfies the unified dynamical balance. An assimilation is carried out with the mediation of nested computation(s) resolving all important topographic and coastal features. The data inversion is carried out by propagating an uncertainty associated with the a priori values of the control parameters to the multigrid model state-space at observation locations. The inverse does not require an adjoint model and is highly practical. In the future, one could consider the idea of having a scheme that corrects for the control parameters defined in each or some of the nested domains, in addition to the outer domain. Such an approach would be desirable in applications where a solution in the nested domains cannot be fully controlled through the OBCs only. A disadvantage of such an approach is that it would result in a discontinuity of the dynamical balance across the domain boundaries. The inverse method discussed in this paper can also become a useful basis for future investigations of data assimilation into models of physical processes occurring on multiple scales. One of our future research directions would include an extension of the method to other models and processes in environmental prediction, monitoring, and planning (Lermusiaux et al. 2007). In addition, other sources of uncertainty could be allowed, for example, to account for the inaccuracies related to nonlinear and frictional effects in the momentum equations and parameterization of the barotropic-to-baroclinic conversions. Work in this direction is currently in progress.

**Acknowledgements** This study was supported by the Office of Naval Research under grants N00014-07-1-0473 (PHILEX), N00014-07-1-0501 (AWACS), N00014-07-1-0241 (core ONR), and N00014-07-1-0241 (QPE) to the Massachusetts Institute of Technology (MIT), with P.F.J. Lermusiaux as principal investigator. We are very grateful to Dr. Janet Sprintall and her team of the Scripps Institution of Oceanography, who provided us with the mooring data from the Panay and the Dipolog straits, instrumental for this study. We also thank the whole PHILEX group of scientists, as well as the team of mooring engineers and technicians involved in the observational program, including the planning, deployment, and recovery of the instruments. This study would not be possible without their efforts and the collected data. The work of Dr. Janet Sprintall and her team was supported by ONR through grant N00014-06-1-0690. Dr. Richard Ray of the Planetary Geodynamics Laboratory at the NASA Goddard Space Flight Center has provided us with the harmonically analyzed TP data. His contribution, critical for this study, is hereby gratefully acknowledged. I would like also to thank Prof. Pierre Lermusiaux (MIT) for his general guidance through the project and many useful discussions and recommendations with regard to the material of this paper. Wayne Leslie and Pat Haley have provided some technical and computer support for this work at MIT. Lastly, the anonymous reviewers of this paper have provided useful criticisms and inputs, which were included in the text and improved the quality and clarity of the presented material.

## Appendix

Index notation

$\mathbf{A} \in \mathbb{C}^{m\times n}$ complex $m \times n$ matrix,

$\mathbf{i}_K \in \mathbb{N}^K$ a set $\mathbf{i}_K = \{i_k\}_{k=1}^K$, $i_k \in \{1, 2, ...\}$,

$(\mathbf{a})_{\mathbf{i}_K} \in \mathbb{C}^K$ complex vector of length $K$ containing the $\mathbf{i}_K$th entries of $\mathbf{a}$, $(\mathbf{a})_{\mathbf{i}_K} = \left[a_{i_1}, a_{i_2}, \ldots, a_{i_K}\right]^T$,

$(\mathbf{A})_{\mathbf{i}_K,\mathbf{j}_L} \in \mathbb{C}^{K\times L}$ complex $K \times L$ matrix containing the entries in the $\mathbf{i}_K$th rows and $\mathbf{j}_L$th columns of matrix $\mathbf{A}$,

$$(\mathbf{A})_{\mathbf{i}_K,\mathbf{j}_L} = \begin{bmatrix} a_{i_1,j_1} & a_{i_1,j_2} & \ldots & a_{i_1,j_L} \\ a_{i_2,j_1} & a_{i_2,j_2} & \ldots & a_{i_2,j_L} \\ \vdots & \ddots & \ldots & \vdots \\ a_{i_K,j_1} & a_{i_K,j_2} & \ldots & a_{i_K,j_L} \end{bmatrix}_{K\times L} .$$

## References

Andersen O, Egbert G, Erofeeva S, Ray S (2006) Mapping nonlinear shallow-water tides: a look at the past and future. Ocean Dyn 56(14):416–429

Barth A, Alvera-Azcrate A, Beckers J-M, Rixen M, Vandenbulcke L (2007) Multigrid state vector for data assimilation in a two-way nested model of the Ligurian sea. J Mar Syst 65:41–59

Bennett A, McIntosh P (1982) Open ocean modeling as an inverse problem: tidal theory. J Phys Oceanogr 12:1004–1018

Bennett AF (1992) Inverse methods in physical oceanography. In: Cambridge monographs on mechanics and applied mathematics. Cambridge University Press, Cambridge

Bennett AF (2002) Inverse modeling of the ocean and atmosphere. Cambridge University Press, Cambridge

Bernard PE, Remacle JF, Legat V (2008) Boundary dicretization for high order discontinuous Galerkin computations of tidal flows around shallow water islands. Int J Numer Methods Fluids. doi:10.1002/fld.1831

Blain CA, Preller RH, Rivera AP (2002) Tidal prediction using the advanced circulation model (ADCIRC) and a relocatable PC-based system. Oceanography 15(1):77–87

Blayo E, Debreu L (2005) Revisiting open boundary conditions from the point of view of characteristic variables. Ocean Model 9(3):231–252

Canizares R, Madsen H, Jensen HR, Vested HJ (2001) Developments in operational shelf sea modelling in Danish waters. Estuar Coast Shelf Sci 53:595–605

Das SK, Lardner RW (1992) Variational parameter estimation for a two-dimensional numerical tidal model. Int J Numer Methods Fluids 15:313–327

Davies AM (1993) A bottom boundary layer-resolving three-dimensional tidal model: a sensitivity study of eddy viscosity formulation. J Phys Oceanogr 23:1437–1453

Davies AM, Jones JE, Xing J (1997) Review of recent developments in tidal hydrodynamic modelling I. Spectral models. J Hydrol Eng ASCE 123:278–292

Dee DP (1995) On-line estimation of error covariance parameters for atmospheric data assimilation. Mon Weather Rev 123:1128–1145

Egbert G, Bennett A, Foreman M (1994) TOPEX/Poseidon tides estimated using a global inverse model. J Geophys Res 99(C12):24821–24852

Egbert GD (1997) Tidal data inversion: interpolation and inference. Prog Oceanogr 40:53–80

Egbert GD, Bennett AF (1996) Data assimilation methods for ocean tides. In: Malanotte-Rizzoli P (ed) Modem approaches to data assimilation in ocean modeling, vol 10. Elsevier, Amsterdam, pp 147–179

Egbert GD, Erofeeva SY (2002) Efficient inverse modeling of barotropic ocean tides. J Atmos Ocean Technol 19:183–204

George K (2007) A depth-averaged tidal numerical model using non-orthogonal curvilinear co-ordinates. Ocean Dyn 57: 363–374

Greenberg DA, Shore JA, Page FH, Dowd M (2005) A finite element circulation model for embayments with drying intertidal areas and its application to the quoddy region of the bay of fundy. Ocean Model 10:211–231

Grenier RR, Luettich RA, Westerin JJ (1995) A comparison of non-linear frictional characteristics of two-dimensional and three-dimensional models of a shallow tidal embayment. J Geophys Res 100:13719–13735

Haley PJ Jr, Lermusiaux PFJ, Robinson AR, Leslie WG, Logutov O, Cossarini G, Liang XS, Moreno P, Ramp SR, Doyle J, Bellingham J, Chavez F, Johnston S (2008) Forecasting and reanalysis in the Monterey Bay/California Current region for autonomous ocean sampling network-II experiment. Deep Sea Res Part II (in press)

Heemink AW, Kloosterhuis H (1990) Data assimilation for non-linear tidal models. Int J Numer Methods Fluids 11(12):1097–1112

Hubbert GD, Preller RH, Posey GDPG, Carroll SN (2001) Software requirements specification for the globally relocatable navy tide/atmosphere modeling system (PCTides). Memorandum Report NRL/MR/7322-01-8266, Naval Research Laboratory, Stennis Space

Jones JE, Davies AM (1996) A high resolution three dimensional model of the M2, M4, M6, S2, N2, K1 and O1 tides in the eastern Irish Sea. Estuar Coast Shelf Sci 42:311–346

Jones JE, Davies AM (2005) An intercomparison between finite difference and finite element (TELEMAC) approaches to modelling west coast of Britain tides. Ocean Dyn 55:178–198

Jones JE, Davies AM (2007a) On the sensitivity of computed higher tidal harmonics to mesh size in a finite element model. Cont Shelf Res 27:1908–1927

Jones JE, Davies AM (2007b) On the sensitivity of tidal residuals off the west coast of Britain to mesh resolution. Cont Shelf Res 27:64–81

Kurapov AL, Egbert GD, Allen JS, Miller RN, Erofeeva SY, Kosro PM (2003) M2 internal tide off Oregon: inferences from data assimilation. J Phys Oceanogr 33:1733–1757

LeProvost C, Genco ML, Lyard F, Vincent P, Canceil P (1994) Spectroscopy of the world ocean tides from a finite element hydrodynamic model. J Geophys Res 99(C12):24777–24798

LeProvost C, Rougier G, Poncet A (1981) Numerical modeling of the harmonic constituents of the tides, with application to the English channel. J Phys Oceanogr 11:1123–1138

LeProvost C, Vincent P (1986) Some tests of precision for a finite element model of ocean tides. J Comput Phys 65:273–291

Lermusiaux PFJ (2006) Uncertainty estimation and prediction for interdisciplinary ocean dynamics. J Comput Phys 217:176–199

Lermusiaux PFJ (2007) Adaptive modeling, adaptive data assimilation and adaptive sampling. Physica D 230:172–196

Lermusiaux PFJ, Chiu CS, Gawarkiewicz GG, Abbot P, Robinson AR, Miller RN, Haley PJ, Leslie WG, Majumdar SJ, Pang A, Lekien F (2006a) Quantifying uncertainities in ocean predictions. Oceanography 19(1):92–105

Lermusiaux PFJ, Malanotte-Rizzoli P, Stammer D, Carton J, Cummings J, Moore AM (2006b) Progress and prospects of U.S. data assimilation in ocean research. Oceanography 19(1):172–183

Lermusiaux PFJ, Haley PJ, Yilmaz NK (2007) Environmental prediction, path planning and adaptive sampling: sensing and modeling for efficient ocean monitoring, management and pollution control. Sea Technol 48(9):3538

Lermusiaux PFJ, Robinson AR (1999) Data assimilation via error subspace statistical estimation. Part I: Theory and schemes. Mon Weather Rev 127(7):1385–1407

Logutov OG (2007) Multi-model fusion and uncertainty estimation for ocean prediction. PhD thesis, Harvard University

Logutov OG, Lermusiaux PFJ (2008) Inverse barotropic tidal estimation for regional ocean applications. Ocean Model 25:17–34

Luettich, Jr. RA, Westerink JJ, Scheffner NW (1992) ADCIRC: an advanced three-dimensional circulation model for shelves coasts and estuaries, report 1: theory and methodology of ADCIRC-2DDI and ADCIRC-3DL. In: Dredging research program technical report DRP-92-6. U.S. Army Engineers Waterways Experiment Station, Vicksburg, p 137

Lynch DR, Hannah CG (1998) Hindcasting the Georges Bank circulation. Part I: Detiding. Cont Shelf Res 18:607–639

McIntosh PC, Bennett AF (1984) Open ocean modeling as an inverse problem: M2 tides in Bass strait. J Phys Oceanogr 14:601–614

Muccino JC, Arango HG, Bennett AF, Chua BS, Cornuelle BD, DiLorenzo E, Egbert GD, Haidvogel D, Levin JC, Luo H, Miller AJ, Moore AM, Zaron ED (2008) The inverse ocean modeling system. II. Applications. J Atm Ocean Tech 25: 1608–1622

Ray RD (2001) Inversion of oceanic tidal currents from measured elevations. J Mar Syst 28:1–18

Robinson AR, Lermusiaux PFJ (2001) Data assimilation in models. In: Encyclopedia of ocean sciences. Academic, London, pp 623–634

Schrama EJO, Ray RD (1994) A preliminary tidal analysis of Topex/Poseidon altimetry. J Geophys Res 99:24799–24808

Smith WHF, Sandwell DT (1997) Global seafloor topography from satellite altimetry and ship depth soundings. Science 277:1957–1962

Snyder R, Sidjabat M, Filloux J (1979) A study of tides, setup and bottom friction in a shallow semi-enclosed basin. part II: Tidal model and comparison with data. J Phys Oceanogr 9:170–188

Sorensen JV, Madsen H (2004) Efficient Kalman filter techniques for the assimilation of tide gauge data in three-dimensional modeling of the North Sea and Baltic Sea system. J Geophys Res 109(C03017):1–14

Walters RA (2005) Coastal ocean models: two useful finite element methods. Cont Shelf Res 25:775–793

Xu J, Lermusiaux PFJ, Haley PJ, Leslie WG, Logutov OG (2008) Spatial and temporal variations in acoustic propagation during PLUSNet-07 exercise in Dabob Bay. In: Proceedings of meetings on acoustics (POMA), vol 4. 155th Meeting Acoustical Society of America, Paris, 29 June–4 July 2008

Xu Z, Hendry RM, Loder JW (2001) Application of a direct inverse data assimilation method to the M2 tide on the Newfoundland and Southern Labrador shelves. J Atmos Ocean Technol 18:665–690